Performance Evaluation of Semi-Active Cab Vibration Isolation of a Wheel Loader Using Fractional-Order PID Controller

Chi-Huan Canh [1], Van-Cuong Bui [2,*], Van-Quynh Le [3]
[1, 2, 3] Faculty of Vehicle and Energy Engineering, Thai Nguyen University of Technology, Thai Nguyen, Vietnam
Email: [1] huanoto@tnut.edu.vn, [2] cuongbui@tnut.edu.vn, [3] lequynh@tnut.edu.vn
*Corresponding Author

***Abstract*—Cab vibration in wheel loaders significantly affects operator ride comfort and working performance. Therefore, this paper presents an approach to improving the vibration isolation performance of the cab in a wheel loader system. First, a three-degree-of-freedom dynamic model is established to characterize the vibration behavior. Subsequently, a semi-active cab vibration isolation (SCVI) system is proposed. To generate the semi-active control force, a fractional-order PID (FOPID) controller is developed. Additionally, a conventional PID controller is considered to facilitate a rigorous and comprehensive evaluation of the proposed control strategy. The grey wolf optimization (GWO) algorithm is employed to tune the controller parameters optimally. Finally, the performance of the proposed system is validated through simulations conducted in the MATLAB/Simulink environment. The results indicate that the proposed SCVI system based on FOPID controller reduces the root mean square (RMS) values of seat acceleration (a_{zs}), cab acceleration (a_{zc}), and cab vibration isolation mount deflection (z_{cf}) by 20.76%, 22.33%, and 48.09%, respectively, compared to the passive cab vibration isolation (PCVI) system, demonstrating a significant improvement in operator ride comfort. These findings contribute to the advancement of cab vibration isolation systems for construction machinery.**

***Keywords*—Semi-Active Cab Vibration Isolation; Wheel Loaders; Cab Vibration; Fractional-Order PID; Grey Wolf Optimization**

I. INTRODUCTION

Wheel loaders are versatile machines widely used in various sectors, including construction, agriculture, mining, and material handling. Due to their ability to operate in harsh and uneven terrains, they are often subjected to severe working conditions. Unlike on-road vehicles, most wheel loaders are not equipped with fully developed suspension systems, which results in significant vibration transmission from the ground through the tires and chassis to the operator's cabin. Consequently, operators are exposed to excessive whole-body vibration, which can adversely affect ride comfort, operational efficiency, and long-term health. Previous studies have shown that prolonged exposure to vibration may lead to musculoskeletal disorders, spinal injuries, and reduced work productivity [1]-[3].

To address the vibration challenges in wheel loaders, early studies have primarily focused on vibration analysis through the development of dynamic models [4]-[6] and the investigation of the influence of structural parameters on vibration characteristics [7], [8]. These studies have made important contributions by providing fundamental insights and a theoretical basis for guiding subsequent research on wheel loader vibration. Building upon these foundations, hydropneumatic suspension systems have been proposed for wheel loaders [9]-[11], with reported results demonstrating significant improvements in vibration attenuation performance. However, the implementation of hydropneumatic suspensions can adversely affect vehicle stability, and their relatively high cost remains a major concern. To overcome these limitations, Bin *et al.* [12] proposed a semi-active seat suspension system. Although the results indicate promising potential in reducing vertical seat vibrations, mitigating vibrations associated with roll and pitch motions remains a significant challenge. Consequently, researchers have increasingly shifted their focus toward enhancing cab vibration isolation performance. Initial efforts in this direction include studies on optimizing the design parameters of cab isolation mounts [13], [14], which provide a solid foundation for structural design and promote the development of improved configurations. On this basis, various cab isolation configurations have been proposed, including rubber mount, hydraulic mount, and pneumatic mount [15]-[18]. In particular, pneumatic mount systems have demonstrated superior vibration reduction performance due to their nonlinear stiffness characteristics and inherent energy dissipation capabilities. Despite these advantages, passive isolation systems are inherently limited in their ability to adapt to varying operating conditions, leading to suboptimal performance under diverse excitation scenarios. Furthermore, certain designs increase system complexity and cost, thereby hindering their practical implementation.

In the context of increasingly stringent requirements for vibration isolation performance and adaptability, semi-active cab isolation systems are considered a promising solution for achieving these objectives. To fully exploit their potential, an appropriate control strategy is essential. Various vibration control strategies for vehicular systems have been proposed, including skyhook control [19], acceleration-driven damping [20], linear quadratic regulator (LQR) control [21], fuzzy logic control [22], proportional–integral–derivative control [23], [24], and hybrid fuzzy–PID approaches [25]-[28]. In general, these control strategies have demonstrated significant effectiveness in improving ride comfort and vibration attenuation. However, fuzzy and fuzzy–PID controllers heavily depend on expert knowledge for rule design and often involve increased computational

complexity. Meanwhile, conventional PID controllers typically exhibit limited performance when dealing with strongly nonlinear and time-varying systems.

Based on the aforementioned literature, it can be observed that although substantial progress has been achieved in the design of passive and semi-active vibration isolation systems, several challenges remain unresolved. Therefore, the development of semi-active cab isolation systems continues to be an open and relevant research direction. In this context, the FOPID controller has emerged as a promising alternative, offering additional degrees of freedom and improved robustness compared to classical control approaches.

The remainder of this paper is organized as follows. Section 2 presents the modeling of the semi-active cab isolation system and the characterization of vibration excitation sources. Section 3 describes the controller design and parameter optimization procedure. Section 4 discusses the obtained results, and finally, Section 5 concludes the paper and outlines directions for future work.

II. WHEEL LOADER MODEL

A. SCVI Model

A wheel loader is a complex multibody system consisting of multiple interconnected subsystems. In terms of its actual structure, the machine body is composed of a front frame and a rear frame. The cab and operator seat are mounted on the rear frame, whereas the front frame accommodates the working implements and the hydraulic actuation system required to perform specific operational tasks. As a result, establishing a comprehensive dynamic model of the entire system is relatively challenging due to the complexity of its structure and interactions. In this context, a quarter-vehicle (single-wheel) model is considered, as this modeling approach is widely adopted in vibration studies for its balance between accuracy and simplicity. Accordingly, the dynamic model of the wheel loader equipped with an SCVI proposed in this study is represented as a multi-layer system, as illustrated in Fig. 1. Specifically, the seat is modeled as a lumped mass (m_s), followed by the cab with mass (m_c), and the main frame with mass (m_f). The formulation of this model still captures the essential dynamic characteristics of the system while maintaining a tractable level of complexity for analysis and control design.

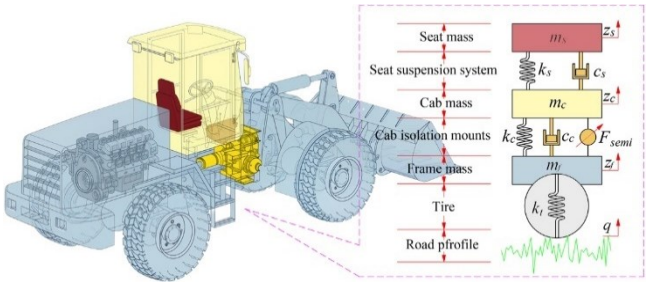

Fig. 1. SCVI model

In Fig. 1, k_s and c_s denote the stiffness and damping coefficient of the seat suspension system, respectively; k_c and c_c represent the stiffness and damping coefficient of the cab isolation system; and k_t corresponds to the equivalent stiffness of the tire. F_{semi} is the semi-active control force generated by the proposed SCVI. Under the excitation of the input vibration source (q), the system exhibits vertical displacements, resulting in the relative motions of the frame, cab, and seat, denoted by z_f, z_c, and z_s, respectively, along the vertical direction.

The equations of motion of the wheel loader illustrated in Fig. 1 can be expressed as follows:

$$\begin{cases} m_s\ddot{z}_s + k_s(z_s - z_c) + c_s(\dot{z}_s - \dot{z}_c) = 0 \\ m_c\ddot{z}_c - k_s(z_s - z_c) - c_s(\dot{z}_s - \dot{z}_c) + \\ k_c(z_c - z_f) + c_c(\dot{z}_c - \dot{z}_f) + F_{semi} = 0 \\ m_f\ddot{z}_f - k_c(z_c - z_f) - c_c(\dot{z}_c - \dot{z}_f) - F_{semi} + \\ k_t(z_f - q) = 0 \end{cases} \quad (1)$$

To represent the system of differential equations in Eq. 1 in state-space form, the state variables can be defined as follows:

$$\begin{cases} X_1(t) = z_s(t) - z_c(t) \\ X_2(t) = z_c(t) - z_f(t) \\ X_3(t) = z_f(t) - q(t) \\ X_4(t) = \dot{z}_s(t) \\ X_5(t) = \dot{z}_c(t) \\ X_6(t) = \dot{q}(t) \end{cases} \quad (2)$$

Let X denote the state variables. The state vector can be expressed in matrix form as follows:

$$\begin{cases} X_i(t) = [X_1(t)\ X_2(t)\ X_3(t)\ X_4(t)\ X_5(t)\ X_6(t)]^T \\ Q(t) = \dot{q}(t) \end{cases} \quad (3)$$

The general form of the state-space equation can be written as:

$$\dot{X}(t) = AX(t) + B_qQ(t) + F_{semi} \quad (4)$$

Where:

$$A = \begin{bmatrix} 0 & 0 & 0 & 1 & -1 & 0 \\ 0 & 0 & 0 & 0 & 1 & -1 \\ 0 & 0 & 0 & 0 & 0 & 1 \\ -\frac{k_s}{m_s} & 0 & 0 & -\frac{c_s}{m_s} & \frac{c_s}{m_s} & 0 \\ \frac{k_s}{m_c} & -\frac{k_s}{m_c} & 0 & \frac{c_s}{m_c} & -\frac{(c_s + c_c)}{m_c} & \frac{c_c}{m_c} \\ 0 & \frac{k_c}{m_f} & -\frac{k_t}{m_f} & 0 & \frac{c_c}{m_f} & -\frac{c_c}{m_f} \end{bmatrix}$$

$$B_q = [0\ 0\ -1\ 0\ 0\ 0]^T$$

$$F_{semi} = [0\ 0\ 0\ 0\ -\frac{F_{semi}}{m_c}\ \frac{F_{semi}}{m_f}]^T$$

B. Input Vibration Source

The primary source of vibration in wheel loaders originates from road surface irregularities, which are inherently stochastic and unpredictable in nature. Therefore, random excitation is commonly employed in vibration studies to realistically represent operating conditions.

Accordingly, to facilitate simulation and evaluate the performance of the proposed SCVI, this study adopts a random road profile model characterized by a specified power spectral density. The corresponding mathematical formulation is expressed as follows:

$$G_q(\tau) = G_q(\tau_0)\left(\frac{\tau}{\tau_0}\right)^{-\vartheta} \tag{5}$$

Where τ denotes the spatial frequency, τ_0 is the reference spatial frequency, and $G_q(\tau_0)$ represents the road roughness coefficient corresponding to the power spectral density evaluated at τ_0; ϑ is the frequency exponent.

Road surface roughness is commonly classified into eight categories, ranging from Grade A to Grade H, according to standardized evaluation criteria. The corresponding pavement roughness characteristics for each grade are summarized in Table 1.

Table 1. Classification of Road Roughness

Road Classes	$G_q(\tau_0)$ (10^{-6} m^3) Geometric Mean	Δ_q (10^{-6} m^3) Geometric Mean
A	16	3.81
B	64	7.61
C	256	51.23
D	1024	30.45
E	4096	60.90
F	16384	121.80
G	65536	243.61
H	262144	487.22

Vehicle speed (v)is an important factor influencing the dynamic response of vibration isolation systems; however, the spatial power spectral density $G_q(\tau_0)$ alone is not sufficient to fully capture this effect. Therefore, the concept of temporal frequency is introduced to provide a more comprehensive representation. The relationship between the temporal frequency (f) and the spatial frequency (n) is expressed as follows:

$$f = vn \tag{6}$$

The time–frequency power spectral density (PSD) of the road excitation can be derived from the spatial PSD using the relationship:

$$G_q(f)\frac{G_q(\tau)}{v} \tag{7}$$

When the frequency index w is assumed to be 2, the expression of the time–frequency PSD can be reformulated as:

$$G_q(f) = 4\pi^2 G_q(\tau_0)\tau_0^2 v \tag{8}$$

By analyzing white noise, the excitation input can be generated as follows:

$$\dot{q(t)} = 2\pi\tau_0\sqrt{G_q(\tau_0)v}\vartheta(t) \tag{9}$$

Since the spectral density is approximately constant in the low-frequency range, a lower cut-off frequency is introduced to more accurately represent the road excitation. By applying the Laplace transform and incorporating the lower cut-off frequency f_0, the formulation can be expressed accordingly.

$$G(j\omega) = \frac{2\pi\tau_0\sqrt{G_q v}}{j\omega + \omega_0} \tag{10}$$

Where $\omega_0 = 2\pi f_0$

The resulting time-domain expression for q, obtained from the Laplace transform, can be written as follows:

$$\dot{q}(t) = 2\pi\tau_0\,\vartheta(t)\sqrt{G_q(\tau_0)v} - 2\pi f_0 q(t) \tag{11}$$

Since wheel loaders typically operate under off-road conditions, a random input of Class E with a vehicle speed of 10 km/h was selected for the investigation. Eq. (11) can be implemented in the Simulink environment as illustrated in Fig. 2, and the corresponding simulation results are presented in Fig. 3.

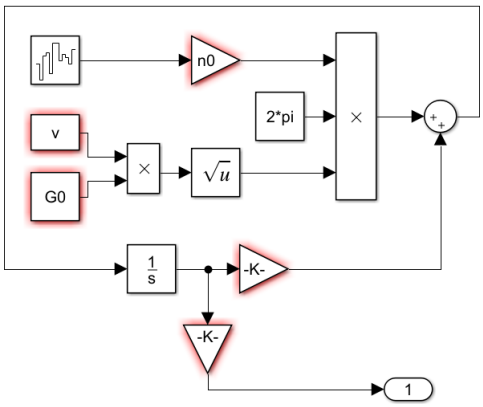

Fig. 2. Random road input model in Simulink

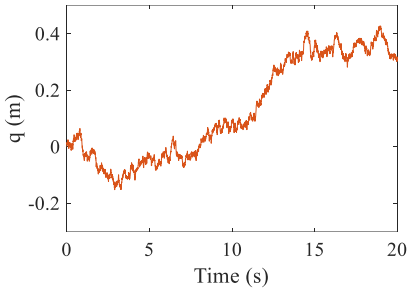

Fig. 3. Simulation results of the road surface profile

III. FOPID CONTROLLER WITH GWO

A. Design of FOPID Controller

To provide a basis for objective comparison and evaluation of the advantages of fractional order control, the conventional PID controller was first implemented for the SCVI system. The time-domain control law of the PID controller is

$$F_{semi} = kp.e(t) + ki\int_0^t e(t)dt + kd\frac{d}{dt}.e(t) \tag{12}$$

Where *kp*, *ki*, and *kd* denote the proportional, integral, and derivative gains, respectively, and *e(t)* is the tracking error.

Building on this framework, an FOPID controller was employed to generate the semi-active control forces for the proposed SCVI system. The FOPID controller generalizes the conventional PID by allowing the integral and derivative actions to take fractional orders, denoted as ϑ and μ, respectively. This additional flexibility enables finer tuning of the dynamic response, resulting in improved vibration suppression and robustness under off-road conditions typical for wheel loaders. The control law of the FOPID controller is given by:

$$F_{semi} = kp.e(t) + ki.D_t^{-\vartheta}.e(t) + kd.D_t^{\mu}.e(t) \quad (13)$$

Where $D_t^{-\vartheta}$ and D_t^{μ} are the fractional integral and derivative operators of orders and, respectively.

The concept of fractional derivatives and integrals is formalized through the generalized operator:

$$D_t^{\alpha} = \begin{cases} \frac{d^{\alpha}}{dt^{\alpha}} & \alpha > 0 \\ 1 & \alpha = 0 \\ \int_{\alpha}^{t} (d\tau)^{-\alpha} & \alpha < 0 \end{cases} \quad (14)$$

This general form allows the operator to represent both differentiation and integration of arbitrary (including non-integer) order α. Three widely used definitions in fractional calculus are then considered for practical implementation

Riemann-Liouville definition:

$$D_t^{\alpha} = \frac{1}{\Gamma(m-\alpha)} \left(\frac{d}{dt}\right)^m \int_{\alpha}^{t} \frac{f(\tau)}{(t-\tau)^{1-m+a}} d\tau \quad (15)$$

Grunwald-Letnikov definition:

$$D_t^{\alpha} = \lim_{h \to 0} h^{\alpha} \sum_{j=0}^{\frac{t-\alpha}{h}} (-1)^j \binom{r}{j} f(t-jh) \quad (16)$$

Caputo definition:

$$D_t^{\alpha} = \frac{1}{\Gamma(m-\alpha)} \int_{\alpha}^{t} \frac{f(\tau)}{(t-\tau)^{1-m+a}} d\tau \quad (17)$$

where $\Gamma(\cdot)$ denotes the Gamma function, and m is the smallest integer greater than α. Among these, the Caputo definition is often preferred in control applications due to its compatibility with initial conditions in the time domain. In practice, fractional-order operators can be implemented using approximation techniques such as the Oustaloup recursive filter.

A fractional-order derivative of order α in the Laplace domain is defined as s^{α}, where s is the Laplace variable. The Oustaloup approximation replaces $s\alpha$ over a specified frequency range [ω_l, ω_h] by a rational function composed of *2N+1* first-order terms:

$$s^{\alpha} \approx k \prod_{i=-N}^{N} \frac{s + \omega_i'}{s + \omega_i} \quad (18)$$

Here, N is the approximation order (number of recursive poles/zeros), ω_i and ω_i' are the distributed poles and zeros, and k is a gain factor ensuring that the magnitude response of the approximation matches the desired s^{α} over the frequency band. The poles and zeros are logarithmically distributed within $[\omega_l, \omega_h]$ according to:

$$\omega_i = \omega_l \left(\frac{\omega_h}{\omega_l}\right)^{\frac{i+N+0.5(1-\alpha)}{2N+1}}$$
$$\omega_i' = \omega_l \left(\frac{\omega_h}{\omega_l}\right)^{\frac{i+N+0.5(1+\alpha)}{2N+1}} \quad (19)$$

The gain factor k is computed as:

$$k = \omega_h^{\alpha} / \prod_{i=-N}^{N} \frac{\omega_i'}{\omega_i} \quad (20)$$

B. Parameter Optimization Using GWO

1. Objective of Parameter Optimization

The performance of both classical PID and FOPID controllers largely depends on the proper selection of controller parameters. For the PID controller, the gains (*kp*, *ki*, *kd*) must be tuned to vibration attenuation. In the case of the FOPID controller, in addition to (*kp*, *ki*, *kd*), the fractional orders (ϑ, μ) also need to be optimized to fully exploit the advantages of fractional-order dynamic.

The main objective of this section is to determine the optimal controller parameters that minimize a defined performance index for the SCVI system, such as the weighted sum of seat acceleration, cab acceleration, and cab vibration isolation mount deflection:

$$minJ = \sqrt{\int_1^T \frac{1}{T} \left(\omega_1 \frac{\ddot{z}_s(X)}{\ddot{z}_{s-pass}} + \omega_2 \frac{\ddot{z}_c(X)}{\ddot{z}_{c-pass}} + \omega_3 \frac{z_{cf}(X)}{z_{cf-pass}} \right) dt} \quad (21)$$

$$X = \begin{cases} [kp, ki, kd] \\ [kp, ki, kd, \vartheta, \mu] \end{cases} \quad (22)$$

$$s.t \begin{cases} \ddot{z}_s(X) < \ddot{z}_{s-pass} \\ \ddot{z}_c(X) < \ddot{z}_{c-pass} \\ z_{cf}(X) < z_{cf-pass} \end{cases} \quad with\ z_{cf} = z_c - z_f \quad (23)$$

where ω_1, ω_2 and ω_3 are weighting factors reflecting the relative importance of vibration reduction, suspension travel, and actuator effort, with their sum normalized to 1. $\ddot{z}_s(X)$, $\ddot{z}_c(X)$, and $z_{cf}(X)$ represent the RMS values for the SCVI system, while $\ddot{z}_{s-pass}, \ddot{z}_{c-pass}$, and $z_{cf-pass}$ represent the RMS values for the PCVI system.

2. GWO Algorithm

The Grey Wolf Optimizer (GWO) was selected in this study due to its superior balance between exploration and exploitation, simple implementation, and strong convergence capability in solving nonlinear and multi-parameter optimization problems [29]-[33]. Compared with conventional algorithms such as Genetic Algorithm (GA), Particle Swarm Optimization (PSO), and Ant Colony

Optimization (ACO), GWO requires fewer control parameters, exhibits higher computational efficiency, and demonstrates better robustness against local optima, making it particularly suitable for the present optimization framework. A key feature of grey wolves is their structured social ranking, which is classified into four levels alpha (α), beta (β), delta (δ), and omega (ω) allowing coordinated behavior during group hunting. This hierarchical organization, combined with their collective mechanisms for encircling, hunting, and attacking prey, enables an effective balance between exploration and exploitation in the search process.

Due to these characteristics, GWO has been widely applied to a variety of single- and multi-objective optimization problems, demonstrating robustness and efficiency in locating global optima. Within the scope of the present study, the GWO algorithm is employed to optimize the parameters of both PID and FOPID controllers for the SCVI system. The algorithm mimics three main phases of grey wolf hunting behavior: encircling the prey, hunting, and attacking the prey, which guide the search agents toward the most promising solutions in the parameter space.

3. *Encircling the Prey*

In the wild, grey wolves surround their prey before initiating an attack. This behavior is emulated in GWO by updating the positions of candidate solutions relative to the best-performing agents. The mathematical model for encircling is expressed as:

$$\begin{cases} D = \left|C\ .\ X_p(t) - X(t)\right| \\ X(t+1) = X_p(t) - A\ .D \\ A = 2\ .A\ .r_1 - a(t) \\ C = 2\ .\ r_2 \end{cases} \tag{24}$$

Where:

- $X_p(t)$ is the position vector of the prey (i.e., the current best solution, α wolf).
- $X(t)$ is the position of the grey wolf (candidate solution),
- r_1, r_2 are random vectors in the range [0,1].
- a decreases linearly from 2 to 0 over iterations to balance exploration and exploitation.

4. *Hunting Behavior*

Grey wolves rely on the three best leaders (α, β, δ) to guide the hunting process. The position of a grey wolf is updated based on its distance from these top wolves:

$$\begin{cases} D_{\alpha i} = \left|C_1\ .\ X_{\alpha i}(t) - X_i(t)\right| \\ D_{\beta i} = \left|C_2\ .\ X_{\beta i}(t) - X_i(t)\right| \\ D_{\delta i} = \left|C_3\ .\ X_{\delta i}(t) - X_i(t)\right| \end{cases} \tag{25}$$

$$\begin{cases} X_{i1} = X_{\alpha i}(t) - a_1\ .\ D_{\alpha i} \\ X_{i2} = X_{\beta i}(t) - a_2\ .\ D_{\beta i} \\ X_{i3} = X_{\delta i}(t) - a_3\ .\ D_{\delta i} \end{cases} \tag{26}$$

$$X_i(t+1) = \frac{X_{i1} + X_{i2} + X_{i3}}{3} \tag{27}$$

5. *Attacking Prey*

As the hunting process progresses, grey wolves gradually converge on the prey, emphasizing exploitation of the promising regions. To reduce the value of a the value of ∂ should converge towards zero.

$$\partial = 2 - \left(\frac{2}{J_{max}}\right) \tag{28}$$

To provide a clear understanding of the GWO process, the algorithmic workflow is illustrated in Fig. 4.

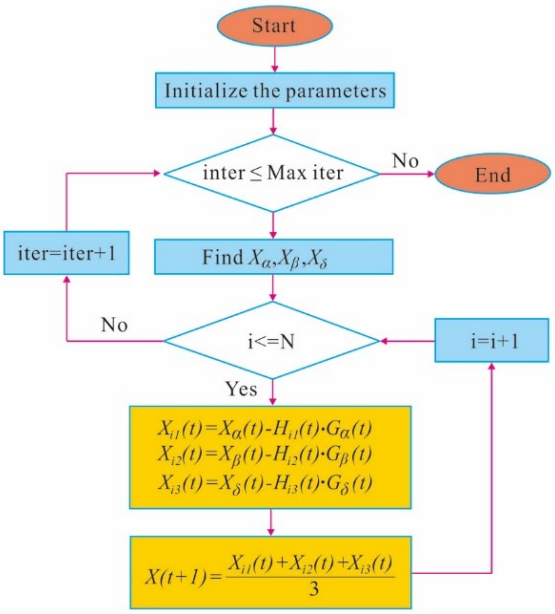

Fig. 4. Flowchart of the GWO algorithm [29]

The parameter optimization of both PID and FOPID controllers was carried out using the GWO algorithm implemented in MATLAB. Based on the input settings summarized in Table 2 and Table 3.

Table 2. GWO algorithm parameter settings

Parameters	Values
GWO size	30
Max iteration	100
a	1
r_1	0.2
r_2	0.25
Lower bound of variables	[0, 0, 0]
Upper bound of variables	[5000, 5000, 5000]

Table 3. Wheel loader dynamic model parameters

Parameters	Unit	Values
m_s	kg	85
m_c	kg	560
m_f	kg	15602
k_s	N/m	2218
c_s	N.s/m	400
k_c	N/m	19235
c_c	N.s/m	700
kt	N/m	392000

Through iterative optimization, the algorithm identified the best combination of controller gains, while also tuning the

fractional orders for the FOPID controller. The resulting optimal parameters, obtained upon convergence, are presented in Table 4.

Table 4. Optimal parameters obtained from GWO optimization

Controller	kp	ki	kd	ϑ	μ
PID	483	26	3590	-	-
FOPID	127	19	4831	0.86	0.91

IV. Assessment of SCVI Performance

The objective of this section is to evaluate the performance of the proposed SCVI system. Numerical simulations were conducted to examine the time-domain responses of the a_{zs}, a_{zc}, and z_{cf}, as illustrated in Fig. 5 to Fig. 7. The corresponding quantitative performance indices are summarized in Table 5. In addition, a frequency-domain assessment was performed to further evaluate system behavior, with the results presented in Fig. 8 to Fig. 10.

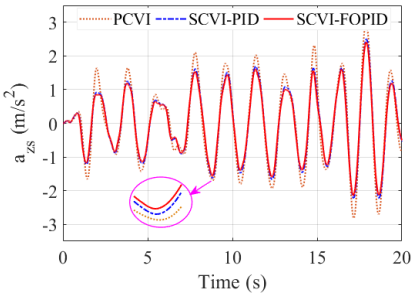

Fig. 5. Comparison of a_{zs} responses

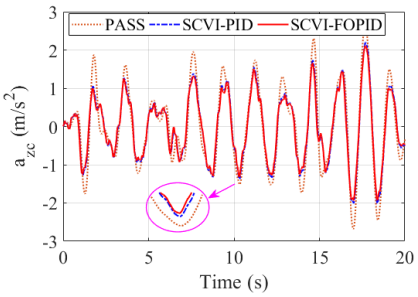

Fig. 6. Comparison of a_{zc} responses

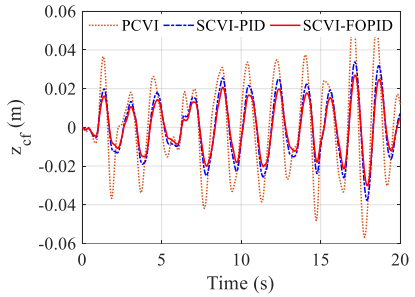

Fig. 7. Comparison of z_{cf} responses

For clarity in the presentation of figures and tables, the semi-active cab vibration isolation system based on the PID controller is denoted as SCVI-PID, while the system employing the fractional-order PID controller is denoted as SCVI-FOPID. The results are presented in Fig. 5 to Fig. 7 clearly demonstrate that the SCVI-FOPID configuration consistently yields lower response amplitudes compared to both the PCVI and the SCVI-PID controller. This indicates a superior vibration attenuation capability of the fractional-order control strategy, particularly under dynamic excitation conditions.

The quantitative results presented in Table 5 further substantiate the aforementioned observations. In particular, the RMS value of azs decreases from 1.2276 m/s² in the PCVI system to 1.0204 m/s² with SCVI-PID, corresponding to a reduction of 16.88%, and is further reduced to 0.9728 m/s² with SCVI-FOPID, achieving a more pronounced reduction of 20.76%.

A similar trend can be observed for azc, where the RMS value declines from 1.085 m/s² in the PCVI configuration to 0.8809 m/s² with SCVI-PID, and further to 0.8427 m/s² with SCVI-FOPID, yielding the maximum reduction of 22.33%.

Furthermore, with respect to the zcf, the SCVI-FOPID system demonstrates the most significant improvement. The RMS value is reduced from 0.0235 m in the PCVI system to 0.0122 m, corresponding to a substantial reduction of 48.09%, which is markedly higher than the 34.89% reduction achieved by the SCVI-PID.

These results clearly indicate that the SCVI-FOPID controller not only enhances ride comfort by effectively reducing vibration levels but also significantly limits cab mount deflection, thereby improving overall system performance and operational stability.

Table 5. Comparison of vibration isolation performance

RMS	Systems				
	PCVI	SCVI-PID	↓(%)	SCVI-FOPIF	↓(%)
azs (m.s2)	1.2276	1.0204	16.88	0.9728	20.76
azc (m.s2)	1.085	0.8809	18.81	0.8427	22.33
zcf (m)	0.0235	0.0153	34.89	0.0122	48.09

To evaluate the effectiveness of the proposed SCVI system in mitigating low-frequency vibrations and shocks, the PSD is analyzed using the Fast Fourier Transform, as illustrated in Fig. 8 to Fig. 10.

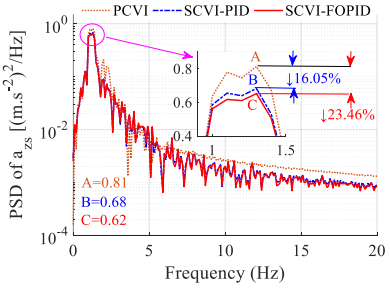

Fig. 8. Comparison of PSD responses of a_{zs}

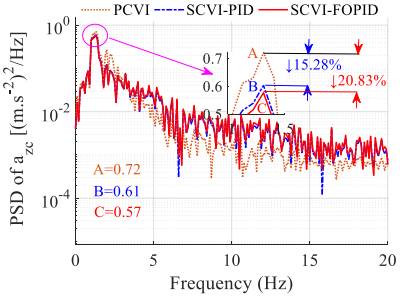

Fig. 9. Comparison of PSD responses of a_{zs}

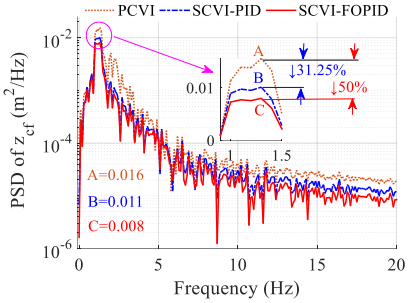

Fig. 10. Comparison of PSD responses of z_{cf}

The results show that vibration energy is primarily concentrated in the low-frequency range (below 5 Hz), which is critical for ride comfort. In this region, both SCVI-PID and SCVI-FOPID significantly reduce the PSD compared to the passive system, with SCVI-FOPID consistently achieving the best performance.

At the resonance peaks, the PSD of a_{zs} is reduced by 16.05% with SCVI-PID and 23.46% with SCVI-FOPID. A similar trend is observed for cab acceleration a_{zc}, with reductions of 15.28% and 20.83%, respectively. For the suspension working space z_{cf}, the reductions are more pronounced, reaching 31.25% with SCVI-PID and up to 50% with SCVI-FOPID.

Overall, the SCVI-FOPID demonstrates superior capability in attenuating low-frequency vibrations and suppressing resonance peaks, thereby enhancing ride comfort and improving system performance compared to both the passive system and the conventional SCVI-PID approach.

V. CONCLUSION

This study introduces an SCVI system for wheel loaders, aiming to enhance vibration isolation performance. The proposed approach employs an FOPID controller to generate the semi-active control force, enabling improved adaptability and robustness under dynamic operating conditions.

The obtained results demonstrate that the proposed SCVI system significantly outperforms the PCVI system within the investigated scenario. In particular, the SCVI strategy effectively reduces vibration amplitudes and improves overall ride comfort and cab stability. Furthermore, frequency-domain analysis based on the PSD confirms that the SCVI system provides substantial attenuation of low-frequency vibrations, which are known to have the most critical impact on operator comfort.

Overall, the findings verify the effectiveness and potential of the FOPID-based semi-active control strategy for practical applications in construction machinery. It should be noted that this study is primarily limited to a theoretical and simulation-based framework. Therefore, future work should focus on extending the model to a full-vehicle dynamic system to capture more complex interactions. In addition, experimental validation, particularly through hardware-in-the-loop (HIL) testing, is recommended to further assess the feasibility and real-world applicability of the proposed control strategy.

ACKNOWLEDGMENT

The authors wish to thank the Thai Nguyen University of Technology for supporting this work.

REFERENCES

[1] X. Zhao, M. Kremb, and C. Schindler, "Assessment of wheel loader vibration on the riding comfort according to ISO standards," *Vehicle System Dynamics*, vol. 51, no. 10, pp. 1548–1567, 2013, https://doi.org/10.1080/00423114.2013.814798.

[2] R. P. Blood, P. W. Rynell, and P. W. Johnson, "Whole-body vibration in heavy equipment operators of a front-end loader: Role of task exposure and tire configuration with and without traction chains," *Journal of Safety Research*, vol. 43, no. 5–6, pp. 357–364, 2012, https://doi.org/10.1016/j.jsr.2012.10.006.

[3] C. Schindler, X. Zhao, and P. Bach, "Reduction of the Vibration Exposure on Wheel Loader Drivers," *ATZoffhighway worldwide*, vol. 9, no. 1, pp. 22–29, 2016, https://doi.org/10.1007/s41321-016-0508-8.

[4] N. L. Pavlov and D. I. Dacova, "A multibody model of a wheel loader with pneumatic boom suspension and proving ground testing," in *IOP Conference Series: Materials Science and Engineering*, 2021, pp. 1–9, https://doi.org/10.1088/1757-899X/1031/1/012009.

[5] C. Y. Chi, S. C. Qin, D. W. Yu, and W. J. Zhang, "The application of pseudo-excitation method to the ride comfort research of wheel-loader," *Applied Mechanics and Materials*, vol. 34–35, pp. 538–543, 2010, https://doi.org/10.4028/www.scientific.net/AMM.34-35.538.

[6] A. Rehnberg and L. Drugge, "Ride comfort simulation of a wheel loader with suspended axles," *International Journal of Vehicle Systems Modelling and Testing*, vol. 3, no. 3, pp. 168–188, 2008, https://doi.org/10.1504/IJVSMT.2008.023836.

[7] N. V. Liem, V. T. P. Thao, and N. T. Trung, "Evaluation of Effects of Wheel Loader Load Condition on Driver Ride Comfort," *International Journal of Future Engineering Innovations*, vol. 2, no. 3, pp. 187–190, 2025, https://doi.org/10.54660/IJFEI.2025.2.3.187-190.

[8] B. V. Cuong, C. C. Huan, L. Van Quynh, and D. T. Binh, "Effects of Design Parameters of Cab's Suspension System on an Agricultural Tractor Ride Comfort," in *Lecture Notes in Networks and Systems*, in Lecture Notes in Networks and Systems, vol. 602 LNNS, pp. 881–886, 2023, https://doi.org/10.1007/978-3-031-22200-9_93.

[9] T. Wei and L. Zhiqiang, "Damping multimode switching control of semiactive suspension for vibration reduction in a wheel loader," *Shock and Vibration*, vol. 2019, pp. 1–12, 2019, https://doi.org/10.1155/2019/4535072.

[10] X. Li, W. Lv, W. Zhang, and H. Zhao, "Research on dynamic behaviors of wheel loaders with different layout of hydropneumatic suspension," *Journal of Vibroengineering*, vol. 19, no. 7, pp. 5388–5404, 2017, https://doi.org/10.21595/jve.2017.18277.

[11] S. Wang, Z. Lu, X. Liu, Y. Cao, and X. Li, "Active control of hydropneumatic suspension parameters of wheel loaders based on road condition identification," *International Journal of Advanced Robotic Systems*, vol. 15, no. 6, pp. 1–13, 2018, https://doi.org/10.1177/1729881418817425.

[12] C. Bin and T. Wei, "Wheel loader seat damping control research based on ADRC," *Advances in Mechanical Engineering*, vol. 16, no. 9, pp. 1–14, Sep. 2024, https://doi.org/10.1177/16878132241281277.

[13] L. Van Quynh, N. T. Duy, N. Van Liem, B. Van Cuong, and L. X. Long, "Optimal Design of Cab's Isolation System for a Single-Drum Vibratory Roller," in *Lecture Notes in Networks and Systems*, in Lecture Notes in Networks and Systems, vol. 178, pp. 619–627, 2021, https://doi.org/10.1007/978-3-030-64719-3_68.

[14] N. T. Dung, B. V. Cuong, L. V. Quynh, and H. Anh Tan, "Optimization of electric vehicle suspension parameters using improved artificial fish swarm algorithm," *Journal of Military Science and Technology*, no. FEE, pp. 191–197, 2024, https://doi.org/10.54939/1859-1043.j.mst.fee.2024.191-197.

[15] L. V. Quynh, L. A. Vu, B. V. Cuong, H. A. Tan, and L. X. Long, "A comparative analysis of ride performance of double-drum vibratory roller with two cab mount systems," in *Lecture Notes in Networks and Systems*, in Lecture Notes in Networks and Systems, vol. 366 LNNS, pp. 19–30, 2022, https://doi.org/10.1007/978-3-030-92574-1_3.

[16] C. C. Huan, B. Van Cuong, L. Van Quynh, N. T. Han, and N. T. T. Hang, "Enhanced ride comfort of wheel loaders using liquid-filled cab vibration isolation: a full-vehicle nonlinear dynamic model," *Vibroengineering Procedia*, vol. 59, pp. 139–146, 2025, https://doi.org/10.21595/vp.2025.25237.

[17] X. Sun, C. Zhang, Q. Fu, H. Zhang, and H. Dong, "Measurement and modelling for harmonic dynamic characteristics of a liquid-filled isolator with a rubber element and high-viscosity silicone oil at low frequency," *Mechanical Systems and Signal Processing*, vol. 140, pp. 1–19, 2020, https://doi.org/10.1016/j.ymssp.2020.106659.

[18] X. Sun, Y. Yang, Q. Fu, and X. Liao, "Time fractional calculus for liquid-path dynamic modelling of an isolator with a rubber element and high-viscosity silicone oil at low frequency," *Meccanica*, vol. 57, no. 11, pp. 2849–2861, 2022, https://doi.org/10.1007/s11012-022-01597-3.

[19] V. C. Bui, X. Yang, Y. Shen, and T. Zhang, "Enhancing Vibration Suppression Efficiency in Hub Motor Drive Vehicle Using Semi-Active ISD Suspension," in *Lecture Notes in Networks and Systems*, in Lecture Notes in Networks and Systems, vol. 1610 LNNS, pp. 260–268, 2026, https://doi.org/10.1007/978-3-032-03856-2_28.

[20] B. V. Cuong, L. V. Quynh, N. T. Dung, and H. A. Tan, "Performance analysis of semi-active suspension in an electric vehicle with acceleration-driven damping," *Journal of Military Science and Technology*, vol. 102, pp. 164–172, 2025, https://doi.org/10.54939/1859-1043.j.mst.102.2025.164-172.

[21] B. V. Cuong, L. V. Quynh, T. M. Huong, N. D. Tan, and V. T. Hien, "Enhancing ride comfort in distributed drive electric vehicle using LQR control for active suspension systems," in *Lecture Notes in Networks and Systems*, in Lecture Notes in Networks and Systems, vol. 1611 LNNS, pp. 312–320, 2025, https://doi.org/10.1007/978-3-032-03859-3_33.

[22] V. Bui and X. Yang, "Control of semi-active inertial suspension system for hub motor driven vehicles," *Proceedings of the Institution of Mechanical Engineers, Part D: Journal of Automobile Engineering*, vol. 240, no. 1, pp. 187–204, 2026, https://doi.org/10.1177/09544070251315857.

[23] N. T. Dung, B. V. Cuong, L. V. Quynh, N. V. Dung, and V. T. Hoang, "Evaluation of ride performance of PID controller in active suspension systems for an electric vehicle," *Vibroengineering Procedia*, vol. 57, pp. 175–181, 2024, https://doi.org/10.21595/vp.2024.24545.

[24] V. Bui, V. Le, A. Ngo, and C. Canh, "Firefly algorithm-based PID optimization for active suspension systems in electric vehicles," *Journal of Fuzzy Systems and Control*, vol. 3, no. 2, pp. 142–148, 2025, https://doi.org/10.59247/jfsc.v3i2.311.

[25] H. A. Tan, B. V. Cuong, N. D. Tan, N. M. Chau, and C. C. Huan, "Improvement of ride quality for a wheel loader with semi-active cab isolation system via fuzzy self tuning of PID controller," *Journal of Military Science and Technology*, no. FEE, pp. 197–203, 2023, https://doi.org/10.54939/1859-1043.j.mst.fee.2023.197-203.

[26] V. Bui, X. Yang, C. Liu, Y. Shen, T. Zhang, and D. Fu, "A Novel Approach to Design and Control of Semi-active Inertial Suspension System for Hub Motor Driven Vehicles," *Journal of Vibration Engineering and Technologies*, vol. 13, no. 6, 2025, https://doi.org/10.1007/s42417-025-01985-5.

[27] V. Bui and V. Le, "Improving ride comfort, stability, and safety of electric vehicles using FFOPID controller," *Proceedings of the Institution of Mechanical Engineers, Part K: Journal of Multi-body Dynamics*, pp. 1–26, 2025, https://doi.org/10.1177/14644193251378235.

[28] V. Bui, V. Le, T. Nguyen, and C. Canh, "Active suspension system control in electric vehicles: A performance comparison of PID, T2FLC, and T2FLC-PID controllers," *Proceedings of the Institution of Mechanical Engineers. Part I: Journal of Systems and Control Engineering*, vol. 240, no. 2, pp. 234–259, 2025, https://doi.org/10.1177/09596518251390695.

[29] M. H. Nadimi-Shahraki, S. Taghian, and S. Mirjalili, "An improved grey wolf optimizer for solving engineering problems," *Expert Systems with Applications*, vol. 166, p. 113917, 2021, https://doi.org/10.1016/j.eswa.2020.113917.

[30] M. Nasir, A. Sadollah, S. Mirjalili, S. A. Mansouri, M. Safaraliev, and A. Rezaee Jordehi, "A Comprehensive Review on Applications of Grey Wolf Optimizer in Energy Systems," *Archives of Computational Methods in Engineering*, vol. 32, no. 4, pp. 2279–2319, 2025, https://doi.org/10.1007/s11831-024-10214-3.

[31] S. K. Verma, S. Yadav, and S. K. Nagar, "Optimization of Fractional Order PID Controller Using Grey Wolf Optimizer," *Journal of Control, Automation and Electrical Systems*, vol. 28, no. 3, pp. 314–322, 2017, https://doi.org/10.1007/s40313-017-0305-3.

[32] Z. Yang and J. Ma, "DEGWO: a decision-enhanced Grey Wolf optimizer," *Soft Computing*, vol. 28, no. 19, pp. 11207–11236, 2024, https://doi.org/10.1007/s00500-024-09878-7.

[33] J. Zhang, Z. Cao, K. Zhang, and J. Chen, "Optimization of Vehicle Suspension Parameters Based on the Multi-Objective Grey Wolf Optimizer," *International Journal of Automotive Technology*, 2026, https://doi.org/10.1007/s12239-026-00473-3.